# Simultaneous SAXS–DSC Study of Multiple Endothermic Behavior in Polyether-Based Polyurethane Block Copolymers

**Jeffrey T. Koberstein***

*Polymer Materials Program, Department of Chemical Engineering, Princeton University, Princeton, New Jersey 08544*

**Thomas P. Russell**

*IBM Almaden Research Center, San Jose, California 95120.* *Received March 22, 1985*

ABSTRACT: The origins of multiple endotherms in segmented polyurethane block copolymers are investigated by simultaneous small-angle X-ray scattering (SAXS) and differential scanning calorimeter (DSC) analyses. The materials examined contain hard segments composed of a 4,4′-methylenediphenyl diisocyanate chain extended with butanediol and soft segments of oxyethylene end-capped poly(oxypropylene). Two distinct endotherms are observed in all materials. A high-temperature endotherm above 200 °C is attributed to melting of microcrystalline hard segments. A lower temperature endotherm is assigned to the onset of microdomain mixing of "noncrystalline" hard and soft microphases that accompanies the microphase separation transition from an ordered to disordered phase. The two endotherm temperatures are found to depend on the annealing temperatures and indirectly on the apparent crystallinity. This behavior is discussed in terms of temperature-induced changes in the hard microdomain structure.

## Introduction

The existence of multiple endotherms has been documented in several studies of the thermal behavior of segmented polyurethane block copolymers.[1-3] In general, three distinct endotherms are observed in differential scanning calorimeter (DSC) experiments. The lowest temperature endotherm ($T_I$) is found at temperatures ca. 20 °C higher than the annealing temperature and has been attributed to a local restructuring of hard-segment units within the hard microdomains. An intermediate temperature endotherm ($T_{II}$), found generally in the range 140–200 °C, has been associated with the destruction of long-range order of an unspecified nature. A higher temperature endotherm ($T_{III}$) observed above 200 °C is generally ascribed to the melting of microcrystalline regions within hard microdomains.

Direct assessment of the morphological origin of polyurethane endotherms has been hampered by the extreme sensitivity of the endothermic response to prior thermal conditioning. In fact, the structure of the materials changes continually during the DSC experiment. Post-scan structural assignments are consequently inappropriate for characterization of the structure present during a particular endotherm.

In the preceding paper[4] it was shown that DSC annealing–quenching studies are useful in characterizing these thermal history effects. The results of the investigation suggested that the $T_{II}$ endotherm was associated with the onset of a microphase separation transition (MST) to a homogeneous phase and that the $T_{III}$ endotherm was the result of melting of microcrystalline hard segments.

The present study examines the behavior of this microphase separation transition by performing structural characterization by small-angle X-ray scattering (SAXS) concurrently with the collection of the DSC thermogram. This is accomplished by the utilization of a DSC cell developed for thermal microscopy, coupled with a synchroton radiation source. Application of this technique to the study of melting and crystallization of polyethylene has already been reported.[5]

## Experimental Section

The polyurethane block copolymers studied are prepared from 4,4′-methylenediphenyl diisocyanate (MDI), butanediol (BD), and poly(oxypropylene glycol). The poly(oxypropylene glycol) ($M_n$ = 2000) is end-capped with 30.4% (w/w) oxyethylene. The samples were kindly supplied by Dr. R. Zdrahala, formerly with Union Carbide Corp., and contain 50–70% (w/w) of the MDI–BD hard segment.[6] They are designated PU-XX where XX refers to the weight percent of the hard segment. Separate determinations of the microdomain structure and thermal properties of these materials will appear shortly.[4,7,8]

The simultaneous SAXS–DSC characterization is accomplished by mounting a sample (~20 mg) into a standard aluminum DSC crucible which is subsequently placed over the thermocouples of a Mettler FP80/FP84 DSC unit. The DSC cell itself contains a 2-mm-diameter hole through which the focused X-ray beam can pass unhindered and is mounted directly in the SAXS apparatus of beam-line I-IV at the Stanford Synchrotron Radiation Laboratory. A schematic diagram of the apparatus is shown in Figure 1. The white radiation emanating from the synchrotron storage ring is focused by means of a float glass mirror and bent, asymmetrically cut Si(111) crystal. The Si crystal monochromator is adjusted to deliver 1.429-Å rays. The incident-beam profile is defined with a number of antiscatter slits to give a cross section of approximately 1 × 1 mm at the sample position. Typical resolution of the apparatus is of the order of 800 Å. The detector is a 1024 pixel EG&G Reticon photodiode array cooled to ca. 190 K and placed several centimeters behind the focal spot of the X-rays. The detector assembly is interfaced to a DEC 1134 computer via CAMAC electronics (see ref 9 for further details). Scintillation detectors placed before and after the sample cell record continuously the incident- and transmitted-beam intensities by diffraction from 10 μm thick Kapton windows inclined at 45° with respect to the incident radiation. Changes in the specimen attenuation factor are consequently monitored continuously. Dried rat-tail tendon is used as a standard to calibrate the position of zero scattering angle.[10]

The DSC unit is scanned at 10 °C/min from 50 to 250 °C and then fast-cooled to the selected annealing temperature and held for approximately 40 min. After annealing, the sample is fast-cooled to 50 °C and immediately scanned to 250 °C at 10 °C/min. Cooling is accomplished with helium gas passed through either ice-water or liquid nitrogen baths. The DSC temperature is calibrated with an indium standard and monitored continuously with a thermocouple placed in the same position. The thermocouple temperature is recorded simultaneously with the SAXS data. During the DSC scan, SAXS profiles are collected and recorded on hard disks at intervals of ~2 °C, corresponding to an accumulated counting time of ~12 s. The corresponding thermograms are plotted and stored on floppy disk by using a Bascom Turner Model 4120 digital recorder.

The torsion braid analyzer (TBA) experiment is carried out with an automated torsion braid analyzer.[11] The sample is coated onto the glass braid by dipping into a 10% solution of the polymer in tetrahydrofuran; it is then dried and held at 150 °C for 10 min to remove residual solvent. A scan up to 240 °C is first made at

* To whom correspondence should be addressed.

0024-9297/86/2219-0714$01.50/0 

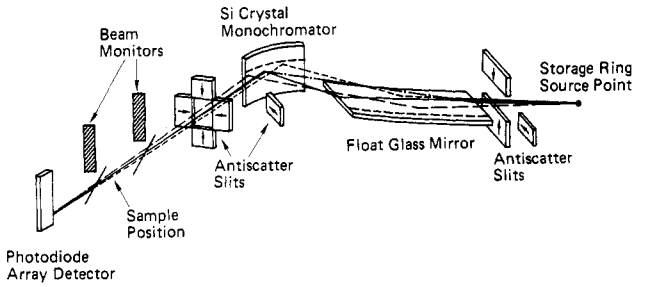


**Figure 1.** Schematic diagram of synchrotron X-ray beam line and apparatus.

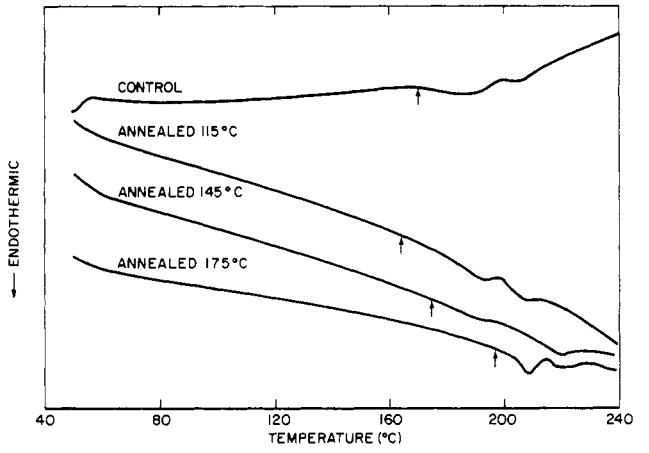


**Figure 2.** DSC thermograms for PU-50 as a function of annealing conditions. The arrows denote the temperature at which the SAXS intensities show a dramatic decrease.

5 °C/min, after which the sample is cooled rapidly (~–5 °C/min) to the annealing temperature of 137 ± 5 °C (below the transition temperature of 160 °C) and held for 40 min. The relative rigidity and loss tangent are calculated continuously during the complete thermal cycle.

## Results and Discussion

DSC thermograms for the PU-50 control (quenched from 250 °C) and for three different annealing conditions appear in Figure 2. Only the $T_{II}$ and $T_{III}$ endotherms are observed for all annealing conditions. The absence of the $T_I$ endotherm results from the particular thermal cycle imposed on the specimens. Previous investigators[3,4] have shown that this endotherm develops rather slowly with time. Independent DSC measurements show that the endotherm appears in these specimens upon extended annealing.[4] The general behavior of the $T_{II}$ and $T_{III}$ endotherms is similar to that reported previously.[1-3] The endotherm temperatures increase with increasing annealing temperatures with the exception of the control sample (effective annealing temperature 250 °C) for which the temperatures are depressed.

An example of the SAXS response (with $h = (4\pi/\lambda) \sin \theta$, where $2\theta$ is the scattering angle and $\lambda$ is the wavelength) during the DSC scan is presented in Figure 3 for the PU-50 specimen annealed at 115 °C. The SAXS curves for other annealing conditions are similar and are not reported. At low temperature, a single broad scattering maximum associated with the interdomain spacing of the microdomains is apparent. As the temperature is raised, the magnitude of the scattering maximum increases and its position shifts to a lower scattering vector. The maximum then disappears completely at higher temperatures. This is illustrated more clearly in Figure 4, wherein the long period ($d = 2\pi/h_{max}$) and DSC heat flux are given as a function of temperature. In all cases studied, the sharp increase in long period is coincident with the onset of the $T_{II}$ endotherm, which was attributed in the preceding paper to the onset of intersegmental mixing during the MST process. Hadziioannou and Skoulios[12] found a similar temperature dependence of the long period at the MST temperature of oriented poly(styrene-*b*-isoprene) diblock copolymers with lamellar microdomain structure. In contrast, Roe et al.[13] found that the long period remained relatively unchanged during the MST in poly(styrene-*b*-butadiene) and diblock and triblock copolymers with spherical microdomain structure.

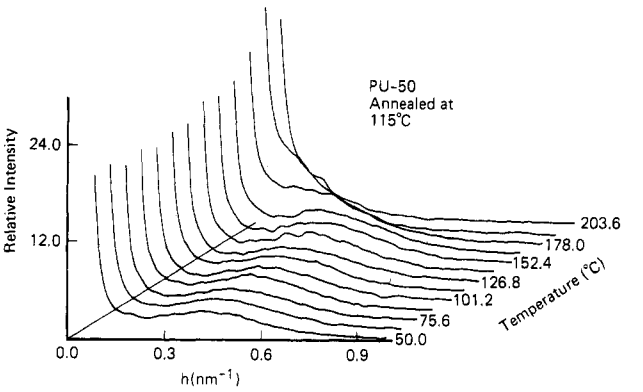


**Figure 3.** Real-time SAXS profiles recorded simultaneously with the DSC scan for PU-50 annealed at 115 °C.

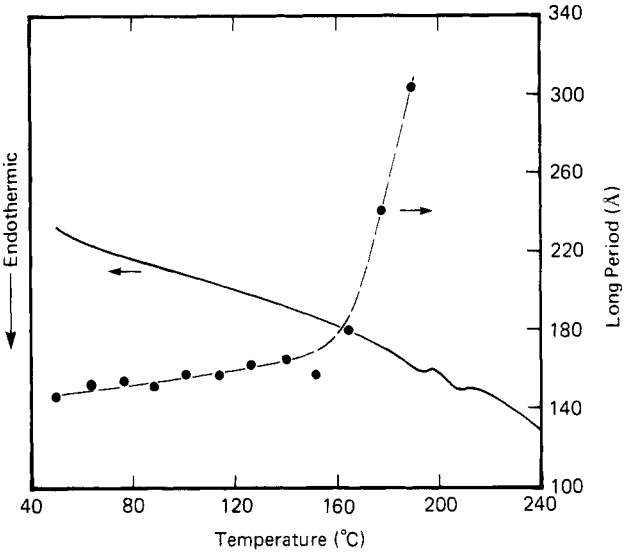


**Figure 4.** Long periods (i.e., interdomain spacings) as a function of temperature for PU-50 annealed at 115 °C. Solid line is the DSC thermogram recorded simultaneously.

Representative results for SAXS determinations of the background fluctuation scattering and diffuse boundary thickness as a function of temperature are presented in Figures 5 and 6, respectively. For this purpose, the background fluctuation scattering was modeled by using plots of ($Ih^4$ vs. $h^4$),[14,15] while the diffuse phase boundary thickness was estimated by using the relation[15,16]

$$\lim_{h\to\infty} I(h) = \frac{K_p}{h^4}\left(1 - \frac{E^2h^2}{12}\right) + I_B \qquad (1)$$

where $I_B$ is the background scattering (assumed to be independent of $h$), $K_p$ is related to the surface-to-volume ratio, and $E$ is the thickness of the linear microphase boundary gradient. The corresponding DSC trace is indicated by the solid lines in Figures 5 and 6.

$I_B$ (Figure 5) begins to rise sharply at ca. 160 °C, coincident with the onset of the $T_{II}$ endotherm in the DSC thermogram. This trend reflects an increase in the local

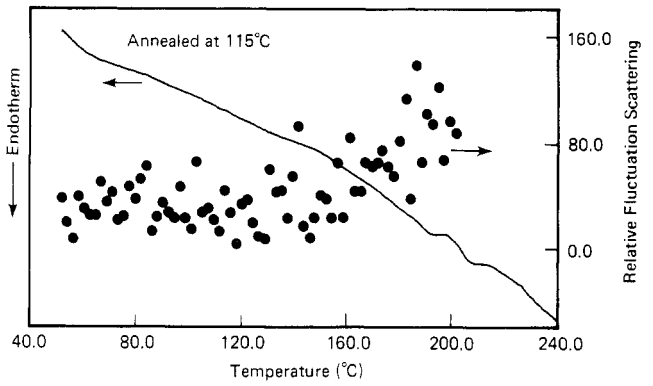


**Figure 5.** Fluctuation scattering as a function of temperature for PU-50 annealed at 115 °C. Solid line is the DSC thermogram recorded simultaneously.

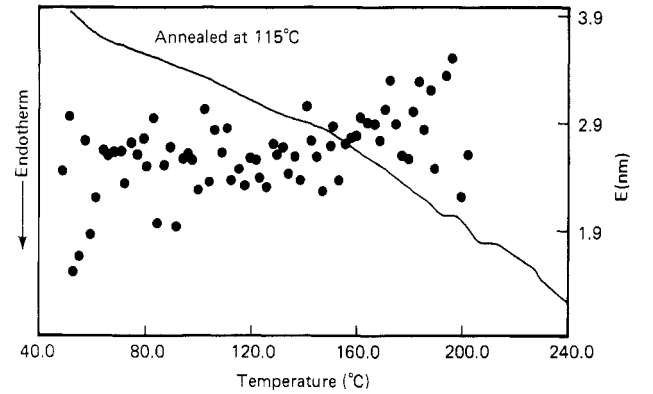


**Figure 6.** Linear diffuse boundary thickness as a function of temperature for PU-50 annealed at 115 °C. Solid line is the DSC thermogram recorded simultaneously.

fluctuations of electron density. Fluctuations of this nature can arise from either of two effects: thermal density fluctuations associated with the finite compressibility of the system or composition fluctuations arising from intersegmental mixing. A sharp rise in the thermal density fluctuations is expected if the specimen undergoes a change of state such as a glass transition.[17] The observed transition at ca. 160 °C, however, is well above the highest anticipated glass-transition temperature (110 °C for pure MDI–BD hard segment[18]). The increase in fluctuation scattering at $T_{II}$ may thus be attributed to increased concentration fluctuations, consistent with the increase in intersegmental mixing expected at the MST.

The diffuse microphase boundary thickness measurements (Figure 6) provide further support for the occurrence of an MST during the $T_{II}$ endotherm. The microdomain boundaries retain a constant thickness ($E \sim 2.5$ nm) up to 150 °C and then broaden slightly to a value of ca. 3.5 nm at 200 °C. Above 200 °C, evaluation of the diffuse boundary thickness is not possible, which is consistent with the idea that the microdomain structure disorders above $T_{II}$. This behavior is again consistent with the results of Hadziioannou and Skoulios,[12] but contrary to those of Roe et al.[13] who found the diffuse boundary thickness to be temperature invariant.

The onset of microphase mixing is also reflected in the temperature dependence of the total integrated scattering intensity, or invariant. The invariant $Q$, corrected for the influence of diffuse microphase boundaries, is given by[19,20]

$$Q = \int_0^\infty \frac{I(h)h^2\,dh}{[1-(E^2h^2/12)]} \qquad (2)$$

The corrected invariant defined by this relation provides

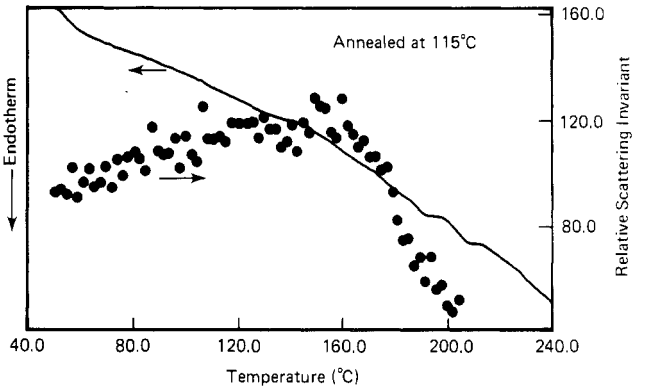


**Figure 7.** Invariant (corrected for diffuse phase boundaries) as a function of temperature for PU-50 annealed at 115 °C. Solid line is the corresponding DSC thermogram.

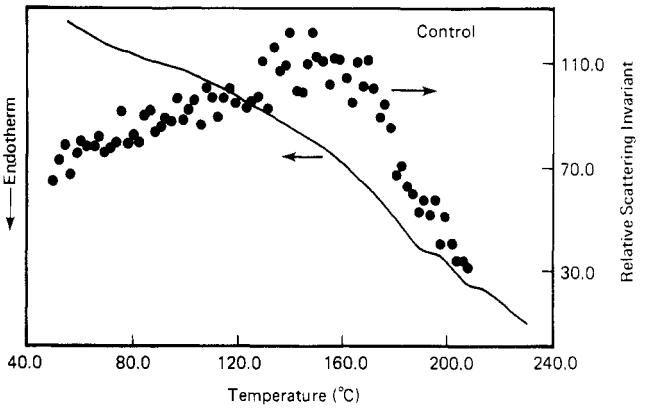


**Figure 8.** Corrected invariant as a function of temperature for PU-50 control (quenched from melt). Solid line is the corresponding DSC thermogram.

an estimate of the degree of mixing within the microphases irrespective of mixing at the microphase boundaries. It is related to the microphase compositions by the expression

$$Q \sim \phi_1(1-\phi_1)(\rho_1-\rho_2)^2 \qquad (3)$$

where $\phi_i$ and $\rho_i$ are the volume fraction and electron density, respectively, of the $i$th microphase. In the event of intersegmental mixing, the electron-density difference between microphases $(\rho_1 - \rho_2)$ will necessarily decrease. Although the term $\phi_1(1-\phi_1)$ may also change, the decrease in $(\rho_1 - \rho_2)$ will generally lead to an associated decrease in the invariant.

The invariant data shown in Figure 7 exhibit a dramatic decrease for temperatures above ca. 160 °C, implying an increase in intersegmental mixing during the $T_{II}$ endotherm. Since the invariant has been corrected for mixing within the diffuse microphase boundary, these results indicate that the compositions of the microphases themselves are changing. Increased mixing is therefore indicated both within the microdomains and at the microdomain boundaries. Essentially identical results are found for the different annealing conditions (Figures 8–10).

The DSC thermograms for samples containing 60% (PU-60) and 70% (PU-70) hard segment appear in Figures 11 and 12, respectively. As in the case of PU-50, the onset of the $T_{II}$ endotherm for all annealing conditions is concurrent with the onset of a drastic reduction in the SAXS invariant (indicated by the arrows in Figures 2, 11, and 12). This is accompanied by increases in the fluctuation scattering, long period (Figure 18), and diffuse microphase boundary thickness. Such behavior provides strong evidence for the occurrence of a microphase mixing transition

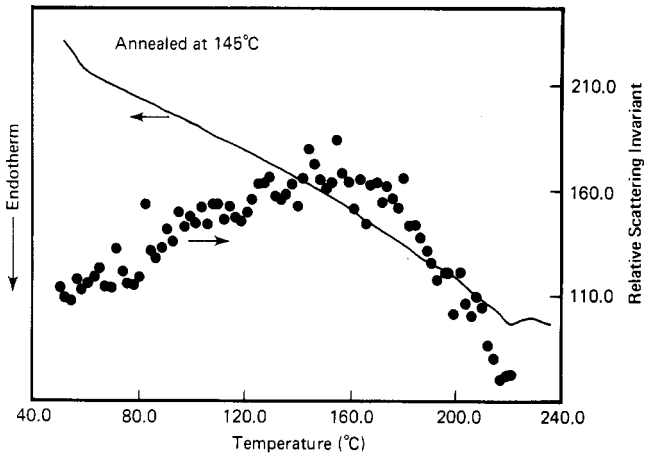


**Figure 9.** Corrected invariant as a function of temperature for PU-50 annealed at 145 °C. Solid line is the corresponding DSC thermogram.

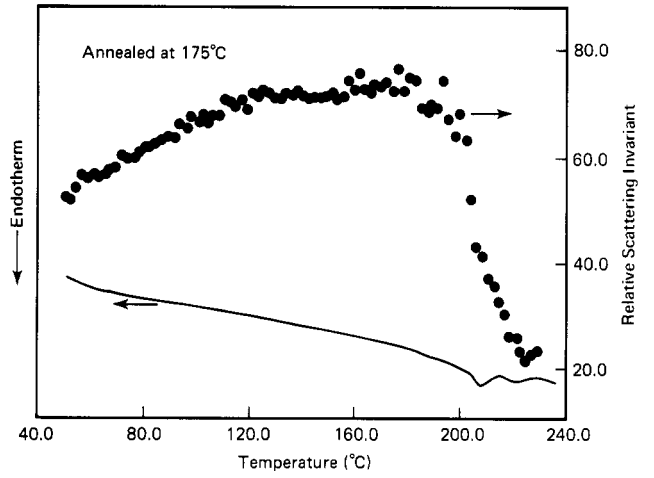


**Figure 10.** Corrected invariant as a function of temperature for PU-50 annealed at 175 °C. Solid line is the corresponding DSC thermogram.

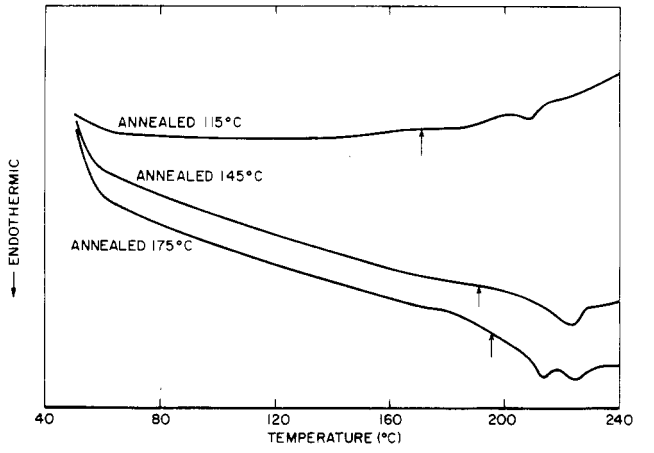


**Figure 11.** DSC thermograms for PU-60 as a function of annealing temperature. The arrows denote the temperatures at which the SAXS invariants show a dramatic decrease.

during the $T_{II}$ endotherm, as was proposed in the preceding paper.[4]

A transition of this nature for polyurethanes was suggested in studies by Wilkes et al.[21,22] on the basis of the results of temperature–time dependent SAXS and mechanical property measurements. Following a quench from the melt to a lower annealing temperature, the modulus, SAXS intensity, and soft-segment glass-transition temperature were all found to increase with time as a result

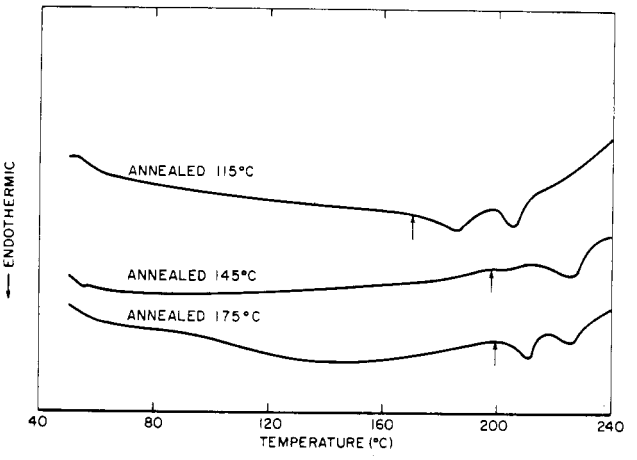


**Figure 12.** DSC thermograms for PU-70 as a function of annealing temperature. The arrows denote the temperatures at which the SAXS invariants show a dramatic decrease.

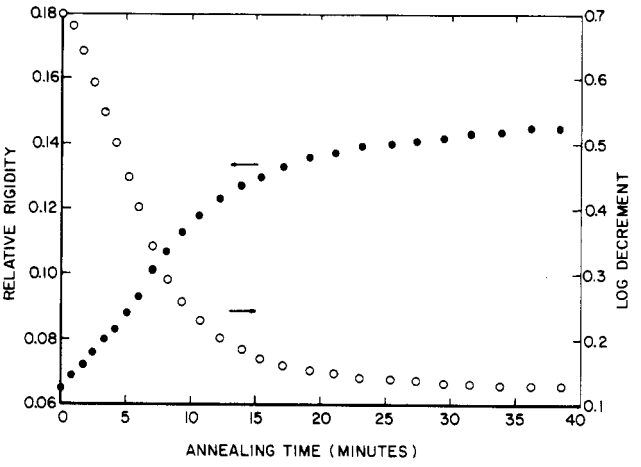


**Figure 13.** Relative rigidity and log decrement from torsional braid analysis as a function of time for PU-50 annealed at 137 ± 5 °C.

of enhanced phase separation. The loss and storage moduli for PU-50 behave in a similar fashion as demonstrated by the torsion braid analysis results in Figure 13. During isothermal annealing after quenching from the melt, the storage modulus (relative rigidity) increases while the loss modulus decreases indicative of an increase in microphase segregation.

The distinction between the model proposed herein and that of Wilkes et al.[20,21] is that in the present work, the microdomain structure disorders according to two apparently distinct processes. First, intermixing of "noncrystalline" hard and soft microphases occurs during the $T_{II}$ endotherm. This is then followed by melting and instantaneous mixing of the microcrystalline hard segments during the $T_{III}$ endotherm. A schematic model representing these morphological transitions appears in Figure 14. This simple model provides a clear explanation for the observation that the softening temperature for these polyurethane specimens is always found between the hard-segment glass-transition and microcrystalline-melting temperatures. Preliminary experiments[8,23] demonstrate that softening coincides with the onset of the $T_{II}$ endotherm, consistent with the hypothesis that the microdomain structure partially disorders at that temperature.

The DSC–annealing study in the preceding paper revealed three different regimes of endotherm response depending on the annealing temperature. In region 1, a $T_{III}$ endotherm was essentially absent, indicating the absence of well-defined crystallinity. Crystalline wide-angle X-ray

**Table I**
**SAXS Transition Temperature, $T_{II}$**

| specimen | wt % hard segment | microphase transition onset temp, °C: annealed at 115 °C | annealed at 145 °C | annealed at 175 °C | control |
|---|---|---|---|---|---|
| PU-50 | 50 | ~164 | ~175 | ~197 | ~170 |
| PU-60 | 60 | ~164 | ~191–198 | ~198 | |
| PU-70 | 70 | ~170 | ~175 | ~205 | |

**Table II**
**Apparent Microcrystalline Melting Temperature, $T_{III}$**

| specimen | wt % hard segment | peak melting temp, °C: annealed at 115 °C | annealed at 145 °C | annealed at 175 °C | control |
|---|---|---|---|---|---|
| PU-50 | 50 | 207 | 218 | 220 | 206 |
| PU-60 | 60 | 209 | 223 | 224 | |
| PU-70 | 70 | 205 | 226 | 226 | |

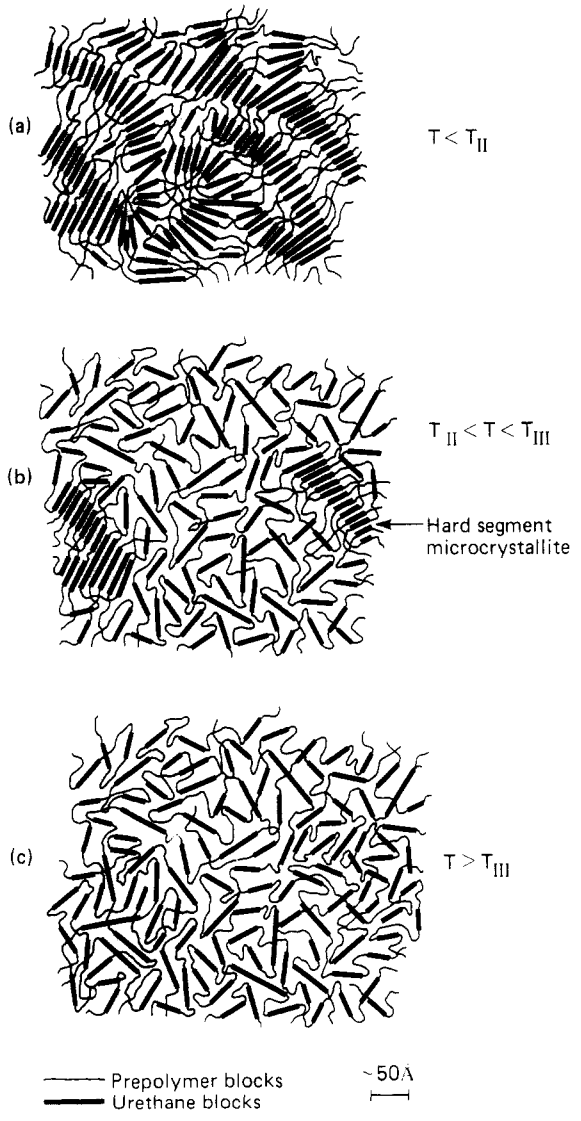


**Figure 14.** Schematic model for the morphological changes that occur during DSC scans of polyurethane elastomers: (a) below the microphase mixing transition temperature; (b) between the microphase mixing temperature and the melting temperature; and (c) above the melting temperature. The microcrystalline hard-segment domains are indicated.

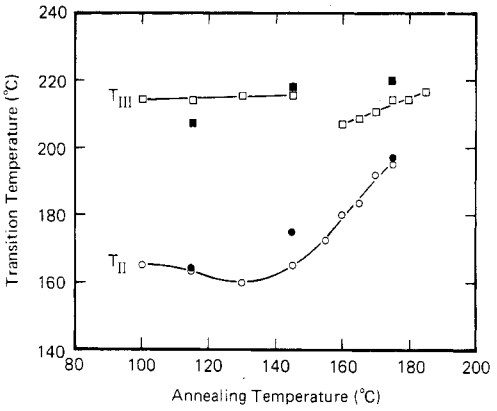


**Figure 15.** Microdomain transition temperatures for PU-50 as a function of annealing temperature. $T_{III}$ peak DSC endotherm temperatures: (□) from preceding article;[4] (■) present data. $T_{II}$ onset temperatures: (○) onset of $T_{II}$ DSC endotherms from preceding article; (●) onset of SAXS invariant falloff.

diffraction peaks are also absent in materials prepared under these same conditions.[23] The MST temperatures for region 1 behavior in the preceding paper were independent of the annealing temperature, but increased with the hard-segment content. (The $T_{II}$ peak endotherm temperatures were approximately 170, 185, and 190 °C for PU-30, PU-50, and PU-70, respectively.[4])

A dependence of the MST temperatures on hard-segment content may be expected. The MST temperature in diblock copolymers, for example, has been shown to depend on the product $\chi N$ as well as the copolymer content,[24] where $\chi$ is the Flory–Huggins interaction parameter and $N$ is the polymerization index. A similar dependence should apply for segmented copolymers. As the hard-segment content varies from 30 to 70%, the average sequence length (calculated by following Peebles[25]) changes from ca. 2.8 to ca. 14.1.[4] If $\chi$ varies inversely with temperature, the effect of the increase in average sequence length would be to raise the MST temperature, as is observed.

A comparison of the preceding DSC results[4] with the SAXS–DSC transitions for PU-50 appears in Figure 15. For this purpose we have estimated $T_{II}$ onset temperatures from the preceding DSC studies for comparison with the SAXS transition onset temperatures. The agreement is especially good considering that the two groups of data were obtained with different scan and quench rates on different instruments. The figure reveals that the simultaneous SAX–DSC data span the range of regions 1 and 2. That is, specimens annealed at 115 °C should be noncrystalline, while those annealed at 145 and 175 °C should exhibit intermediate and near maximum levels of crystallinity, respectively.

The data in Tables I and II show clearly that the level of crystallinity within these regions controls both the $T_{II}$ and $T_{III}$ temperatures and therefore the softening characteristics (i.e., at $T_{II}$), as alluded to previously (even though softening occurs prior to melting). An increase in crystallinity (i.e., increase in annealing temperature) results in an elevation of both the $T_{II}$ and $T_{III}$ temperatures. From

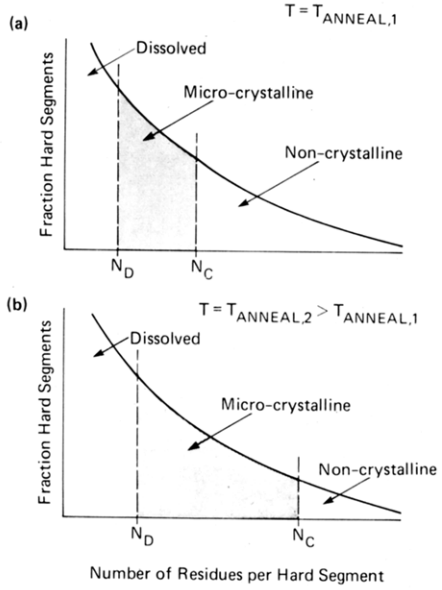


**Figure 16.** Possible partitioning of the hard-segment sequence length distribution as a function of annealing temperature for region 2 behavior. Segments with lengths less than $N_D$ are most likely dissolved within the soft microphase. Segments with lengths between $N_D$ and $N_C$ have the highest probability for crystallization. Crystallization of segments with lengths greater than $N_C$ is hindered due to morphological constraints.

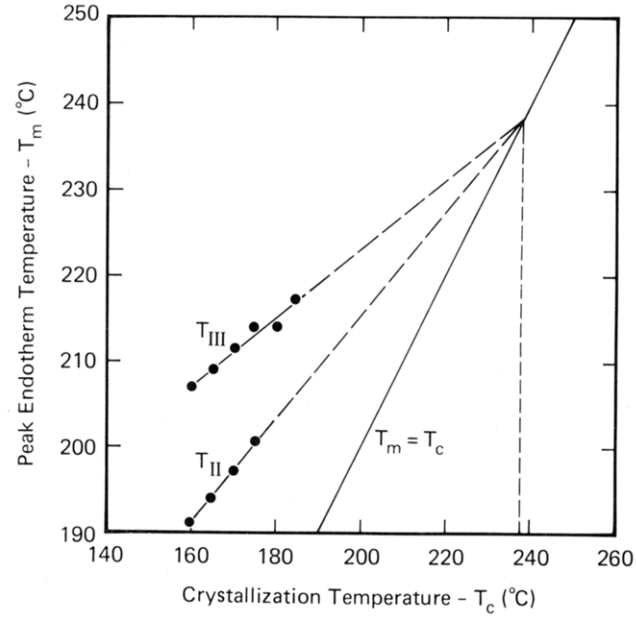


**Figure 17.** Peak endotherm temperatures as a function of annealing (i.e., crystallization) temperature for PU-50. Data taken from preceding article.[4]

the preceding discussion, elevation of $T_{II}$ would imply an increase in the average length of the segregated "noncrystalline" hard segments.

One scheme by which this increase in length may be accommodated while still increasing the overall level of crystallinity is pictured in Figure 16. This situation would arise if there is a tendency for intermediate-length sequences to crystallize preferentially. As the annealing temperature is raised, the critical length for hard-segment dissolution ($N_D$) increases, and increased mobilities permit crystallization of successively longer hard-segment sequences. The average molecular weight of the "noncrystalline" hard segments consequently increases, which can account for the observed elevation in the MST temperature.

Although crystallization of shorter sequences may at first appear counterintuitive, this possibility becomes more feasible when the morphological constraints for crystallization are considered. Within region 2, for example, crystallization must occur within the confines of the preexistent microdomain structure. If the microdomain model of Koberstein and Stein[20] is approximate, the thickness of the microdomain is limited by incorporation of short hard segments within the microdomain. This forces longer sequences to take on coiled rather than extended configurations. The severe morphological constraints on these longer chains confined within the thin microdomains might then impede their crystallization. Indeed this model accounts for the low level of hard-segment crystallinity generally observed in unoriented polyurethane elastomers.

This simple model also accounts for the elevation in the $T_{III}$ transition as the annealing temperature increases. The Koberstein–Stein model[20] predicts that the microdomain thickness is roughly proportional to the critical sequence length ($N_D$) for dissolution of hard segments within the soft microphase. Thus as $N_D$ increases, the microdomains (i.e., crystals) thicken, and the melting temperature is expected to increase, as is found for conventional semicrystalline homopolymers.[26] In the latter case, however, the increase in crystal thickness is related to the thermodynamics of crystallization in a homogeneous fluid rather than to the morphological constraints and thermodynamics of microphase separation.

Although it is not clear which effect is dominant for the polyurethanes, the region 2 data for $T_{III}$[4] does conform to the behavior expected for semicrystalline homopolymers, as evidenced by the Hoffman–Weeks plot in Figure 17. Although an extrapolation to 0 heating rate has not been applied, the data does extrapolate linearly to an apparent equilibrium melting point of ca. 239 °C. Furthermore, the long-period data in Figure 18 provide indirect evidence for microdomain thickening as the annealing temperature is increased from 115 to 175 °C. In all cases, the long period increases with the annealing temperature, implying a proportionate increase in microdomain (i.e., crystal) thickness. The magnitude of the long-period increase also correlates qualitatively with the relative elevation in $T_{III}$ (Table II), being generally larger between 115 and 145 °C than between 145 and 175 °C.

One interesting feature of Figure 17 is that the $T_{II}$ peak temperatures in region 2 also conform to a linear $T_m$ vs. $T_c$ dependence and extrapolate to the same apparent equilibrium melting temperature found for $T_{III}$. This behavior may be coincidental but may suggest the existence of a second disordered crystal structure with a melting point at $T_{II}$. Recent studies have demonstrated the existence of polymorphs in heat-set[27] and solution-cast specimens[28] and have implied their existence in pure MDI–BD hard segments.[29] For this reason, we have purposely qualified the term "noncrystalline" by quotation marks, leaving open the possibility that these hard segments may actually be highly disordered crystals. Within region 1, the microdomains do not contain disordered crystals, as indicated by the referenced diffraction experiments. Within region 2, however, this same statement cannot be made. The SAXS–DSC experiments presented herein cannot distinguish whether the $T_{II}$ peaks within region 2 are of a disordered crystalline or noncrystalline nature.

The prevalence for polymorphism, however, would not significantly alter our interpretation of the present results. If the so-called "noncrystalline" hard segments actually

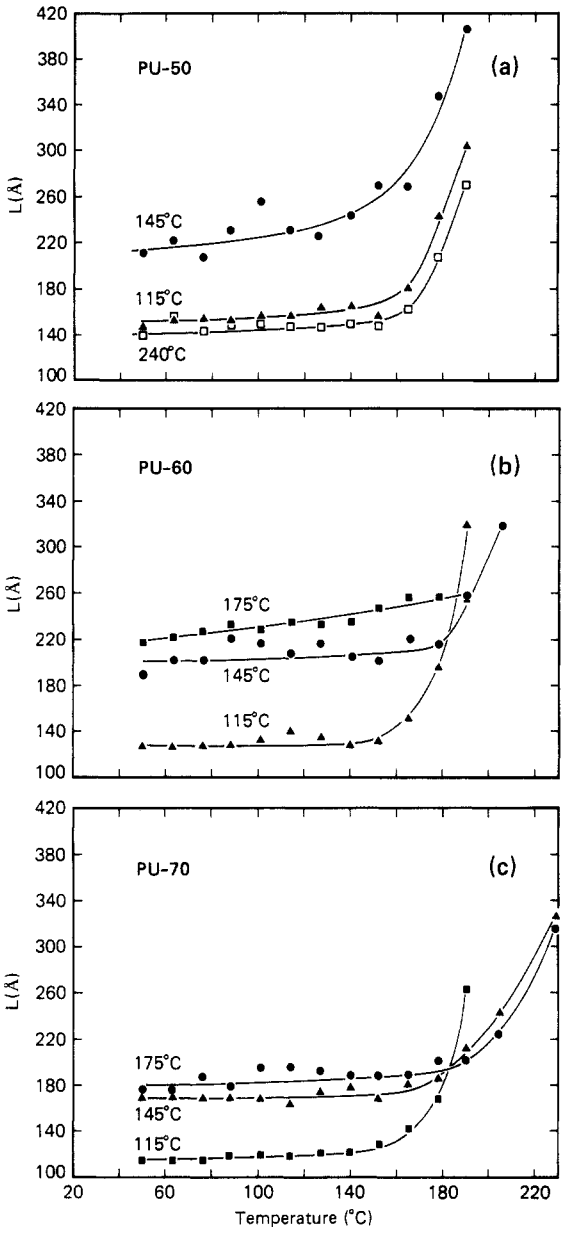


**Figure 18.** Long periods as a function of temperature measured during a DSC experiment. Temperature labels refer to annealing conditions: (a) PU-50; (b) PU-60; (c) PU-70.

exist as "disordered" crystals, they would simply melt and spontaneously mix at $T_{II}$, in much the same manner as the microcrystals melt and mix at $T_{III}$. The previous arguments concerning either crystal thickening or partitioning according to sequence length would still account for the observed trends in $T_{II}$ and $T_{III}$ with annealing temperature.

Wide-angle X-ray diffraction (WAXD) and simultaneous SAXS–WAXD–DSC experiments are currently in progress in order to resolve these issues.

## Conclusions

Simultaneous SAXS–DSC measurements of the multiple endotherms occurring in polyurethane elastomers clearly show that the intermediate-temperature ($T_{II}$) endotherm is associated with the onset of partial intersegmental mixing. This microphase mixing transition is evidenced by dramatic increases in the diffuse microphase boundary thickness, long period and fluctuation scattering, and a drastic decrease in the SAXS invariant. Under all thermal annealing conditions, the transition is found to occur prior to melting of microcrystalline hard-segment sequences during the $T_{III}$ endotherm. The temperatures corresponding to the microcrystalline melting and microphase disorder endotherms increase with both the hard-segment content and annealing temperature.

**Acknowledgment.** Some of the materials incorporated in this work were developed at the Stanford Synchrotron Radiation Laboratory with the financial support of the National Science Foundation (DMR-77-27489) in cooperation with the Department of Energy. The project is supported by NSF grants DMR-8105612 from the Polymers Program and INT-8116066 and a grant from the Dow Chemical Co. Foundation. We wish to thank Dr. L. M. Leung, Dr. I. Gancarz, and A. Galambos for their assistance in preparing samples and conducting some of the experiments. Also, we are grateful to M. Aronhime for his assistance with the TBA measurements.

**Registry No.** (MDI)·(BD)·(methyloxirane)·(oxirane) (copolymer), 34407-15-3.

## References and Notes

(1) Seymour, R. W.; Cooper, S. L. *Macromolecules* **1973**, *6*, 48.
(2) Jacques, C. H. M. "Polymer Alloys"; Klempner, D. K.; Frisch, K. C., Eds.; Plenum Press: New York, 1977; p 287.
(3) Hesketh, T. R.; Van Bogart, J. W. C.; Cooper, S. L. *Polym. Eng. Sci.* **1980**, *20*(1), 190.
(4) Leung, L. M.; Koberstein, J. T. *Macromolecules*, preceding paper in this issue.
(5) Russell, T. P.; Koberstein, J. T. *J. Polym. Sci., Polym. Phys. Ed.* **1985**, *23*, 1109.
(6) Zdrahala, R. J.; Critchfield, F. E.; Gerkin, R. M.; Hager, S. L. *J. Elastomers Plast.* **1980**, *12*, 184.
(7) Leung, L. M.; Koberstein, J. T. *J. Polym. Sci., Polym. Phys. Ed.* **1985**, *23*, 1883.
(8) Leung, L. M.; Galambos, A.; Koberstein, J. T., unpublished data.
(9) Stephenson, G. B. Ph.D. Dissertation, Stanford University, 1982. (Report No. 82/05, Stanford Synchrotron Radiation Laboratory, Stanford, CA.)
(10) Russell, T. P. *J. Appl. Crystallogr.* **1983**, *16*, 437.
(11) Gillham, J. K. "Developments in Polymer Characterization-3"; Dawkins, J. V., Ed.; Applied Science: London, 1982; p 159.
(12) Hadziioannou, G.; Skoulios, A. *Macromolecules* **1982**, *15*, 271.
(13) Roe, R. J.; Fishkis, M.; Chang, J. C. *Macromolecules* **1981**, *14*, 1091.
(14) Bonart, R.; Müller, E. H. *J. Macromol. Sci., Phys.* **1974**, *B10*, 177.
(15) Koberstein, J. T.; Morra, B.; Stein, R. S. *J. Appl. Crystallogr.* **1980**, *13*, 34.
(16) Ruland, W. *J. Appl. Crystallogr.* **1971**, *4*, 70.
(17) Wendorff, J. H.; Fisher, E. W. *Kolloid Z. Z. Polym.* **1973**, *251*, 876.
(18) MacKnight, W. J.; Yang, M.; Kajiyama, T. *Polym. Prepr. (Am. Chem. Soc., Div. Polym. Chem.)* **1968**, *9*(1), 860.
(19) Bonart, R.; Müller, E. H. *J. Macromol. Sci., Phys.* **1974**, *B10*, 345.
(20) Koberstein, J. T.; Stein, R. S. *J. Polym. Sci., Polym. Phys. Ed.* **1983**, *21*, 1439.
(21) Wilkes, G. L.; Wildnauer, R. *J. Appl. Phys.* **1975**, *46*, 4148.
(22) Wilkes, G. L.; Emerson, J. A. *J. Appl. Phys.* **1976**, *47*, 4261.
(23) Galambos, A.; Koberstein, J. T. *Bull. Am. Phys. Soc.* **1985**, *30*(3), 444.
(24) Leibler, L. *Macromolecules* **1980**, *13*, 1602.
(25) Peebles, L. H., Jr. *Macromolecules* **1976**, *9*, 58.
(26) Hoffman, J. D.; Davis, G. T.; Lauritzen, J. I., Jr. "Treatise on Solid State Chemistry"; Hannay, N. B., Ed.; Plenum Press; New York, 1976; Vol. 3.
(27) Blackwell, J.; Lee, C. D. *J. Polym. Sci., Polym. Phys. Ed.* **1984**, *22*, 759.
(28) Briber, R. M.; Thomas, E. L. *J. Macromol. Sci., Phys.* **1983**, *B22*, 509.
(29) Macosko, C. W., private communication.